Eye-safe diode laser Doppler lidar with a MEMS beam-scanner

Hu, Qi; Pedersen, Christian; Rodrigo, Peter John

Published in:
Optics Express

Link to article, DOI:
10.1364/oe.24.001934

Publication date:
2016

Document Version
Publisher's PDF, also known as Version of record

Eye-safe diode laser Doppler lidar with a MEMS beam-scanner

Qi Hu,[1,2] Christian Pedersen,[1] and Peter John Rodrigo[1,*]

[1]*DTU Fotonik, Department of Photonics Engineering, Technical University of Denmark, 4000 Roskilde, Denmark*
[2]*Windar Photonics A/S, Helgeshøj Alle 16-18, 2630 Taastrup, Denmark*
[*]*pejr@fotonik.dtu.dk*

Abstract: We present a novel Doppler lidar that employs a cw diode laser operating at 1.5 μm and a micro-electro-mechanical-system scanning mirror (MEMS-SM). In this work, two functionalities of the lidar system are demonstrated. Firstly, we describe the capability to effectively steer the lidar probe beam to multiple optical transceivers along separate lines-of-sight. The beam steering functionality is demonstrated using four lines-of-sight – each at an angle of 18° with respect to their symmetry axis. Secondly, we demonstrate the ability to spatially dither the beam focus to reduce the mean irradiance at the probing distance (R = 60 m) of each line-of-sight – relevant for meeting eye-safety requirements. The switching time of the MEMS-SM is measured to be in the order of a few milliseconds. Time-shared (0.25 s per line-of-sight) radial wind speed measurements at 50 Hz data rate are experimentally demonstrated. Spatial dithering of the beam focus is also implemented using a spiral scan trajectory resulting in a 16 dB reduction of beam focus mean irradiance.

OCIS codes: (010.3640) Lidar; (140.5960) Semiconductor lasers; (230.4685) Optical microelectromechanical devices.

References

1. R. S. Hansen and C. Pedersen, "All semiconductor laser Doppler anemometer at 1.55 μm," Opt. Express **16**(22), 18288–18295 (2008).
2. P. J. Rodrigo and C. Pedersen, "Field performance of an all-semiconductor laser coherent Doppler lidar," Opt. Lett. **37**(12), 2277–2279 (2012).
3. P. J. Rodrigo, T. F. Iversen, Q. Hu, and C. Pedersen, "Diode laser lidar wind velocity sensor using a liquid-crystal retarder for non-mechanical beam-steering," Opt. Express **22**(22), 26674–26679 (2014).
4. K. A. Kragh, M. H. Hansen, and T. Mikkelsen, "Precision and shortcomings of yaw error estimation using spinner-based light detection and ranging," Wind Energy (Chichester Engl.) **16**(3), 353–366 (2013).
5. D. Schlipf, D. J. Schlipf, and M. Kühn, "Nonlinear model predictive control of wind turbines using LIDAR," Wind Energy (Chichester Engl.) **16**(7), 1107–1129 (2013).
6. T. Mikkelsen, J. Mann, M. Courtney, and M. Sjøholm, "Windscanner: 3-D wind and turbulence measurements from three steerable Doppler lidars," in *IOP Conf. Ser.: Earth Environ. Sci.* (2008), paper 012018.
7. T. Mikkelsen, N. Angelou, K. Hansen, M. Sjöholm, M. Harris, C. Slinger, P. Hadley, R. Scullion, G. Ellis, and G. Vives, "A spinner-integrated wind lidar for enhanced wind turbine control," Wind Energy (Chichester Engl.) **16**(4), 625–643 (2013).
8. S. T. S. Holmström, U. Baran, and H. Urey, "MEMS laser scanners: a review," J. Microelectromech. Syst. **23**(2), 259–275 (2014).
9. L. Mol, L. A. Rocha, E. Cretu, and R. F. Wolffenbuttel, "Fast step-response settling of microelectrostatic actuators operated at low air pressure using input shaping," J. Micromech. Microeng. **19**(7), 074020 (2009).
10. M. Harris, S. M. Stone, and A. Lewin, "Lidar Mean Power Reduction," U.S. Patent 20110149363 (2011).

1. Introduction

Since 1970s, coherent laser radars (also known as Doppler lidars) for wind velocimetry have been mostly limited to scientific use due to lack of inexpensive laser sources with appropriate optical power, wavelength and coherence. The potential of laser based wind sensors in industrial applications, e.g. in wind energy industry, has been greatly enhanced by the use of

#255741 Received 16 Dec 2015; revised 19 Jan 2016; accepted 21 Jan 2016; published 25 Jan 2016

cost-efficient semiconductor laser sources operating at 1.5 μm [1,2]. Previously, we have improved our diode laser based lidar wind sensor by incorporating an electronically controlled liquid-crystal retarder (LCR) as means to switch the beam direction between two lines-of-sight (LOS) [3]. This equips the low-cost lidar with the capability to measure not only the magnitude but also the direction of a 2D wind vector, assuming a relatively laminar wind flow. It makes the lidar system useful for applications like wind turbine yaw control [4]. By increasing the number of LOS and hence the velocity components that can be obtained, the lidar functionality can extend to wind shear measurement or perhaps even blade pitch control of wind turbines [5]. Existing lidar scanning systems either rely on a mechanical scanning head [6] or integrate the lidar inside the turbine spinning hub [7]. Due to mechanical wear and tear, the scanning head has a limited operational lifetime, making it undesirable from an industrial point of view. In principle, the spinning lidar [7] does not necessarily require any mechanical beam-scanner from the lidar itself, but the lidar's integration inside the spinning hub is more complicated than the installation of nacelle-mounted lidars that are easier to retrofit in existing turbines. One could use a variant of the LCR based wind lidar [3] to generate more than two LOS. However, the method entails that the transmitted beam passes through multiple LCR units – thus increasing optical insertion loss and wavefront aberration that ultimately degrade the lidar's sensitivity (signal-to-noise ratio).

In this work, we demonstrate an alternative solution to create multiple LOS in our 1.5 μm semiconductor laser lidar system. The proposed method has the advantage of simplicity, low insertion loss, low power consumption, and wavelength- and polarization-independent operation. Only one optical switching device is utilized which leads to reduced footprint and low cost for the lidar system. This novel method relies on a single dual-axis micro-electro-mechanical-system scanning mirror (MEMS-SM) [8]. The use of a two-axis MEMS-SM enables angular deflection of the lidar beam (± 15° optical deflection for each axis) to several LOS – the number of LOS is limited by the size of optical transceivers that can fit within a given footprint. The MEMS-SM is specified with >1 billion switch cycles of operation. Furthermore, the MEMS-SM can be used to spatially dither the beam and potentially reduce the mean irradiance down to a prescribed eye-safe level at the focal plane. In the following sections, we describe the two MEMS-SM functionalities and demonstrate the operation of the lidar system by measuring multiple (four LOS) radial wind speed components.

2. Lidar configuration based on a MEMS scanning mirror

Figure 1(a) shows the geometrical configuration of the probing directions in our "multiple-beam" lidar system if mounted on the nacelle of a wind turbine to preview the approaching wind. The lidar transmitted beam is time-shared among the four LOS. Speed component along each LOS is measured for 0.25 s in each cycle in our demonstration. The schematic diagram of the lidar system itself is shown in Fig. 1(b) where only two of the four LOS are shown. A fiber-coupled cw diode laser with ~500 mW of optical power operating at wavelength λ = 1.5 μm is used. The laser beam is transmitted through a single-mode fiber into an optical circulator that taps a tiny fraction (~0.1%) of the laser power and directs it to the detector as a local oscillator. A Doppler shifted backscattered radiation from aerosol in the probe volume coherently mixes with the local oscillator resulting in a detector beat signal that oscillates at a mean Doppler shift frequency f_D. The field-programmable gate array (FPGA) board calculates the power spectral density (PSD) from 512-point time series (100 MHz sampling) of the ac-coupled detector signal. Averages of the spectra are produced to estimate at 50 Hz rate the radial wind speed v_{LOS}:

$$v_{LOS} = \frac{\lambda}{2} f_D. \quad (1)$$

#255741 Received 16 Dec 2015; revised 19 Jan 2016; accepted 21 Jan 2016; published 25 Jan 2016

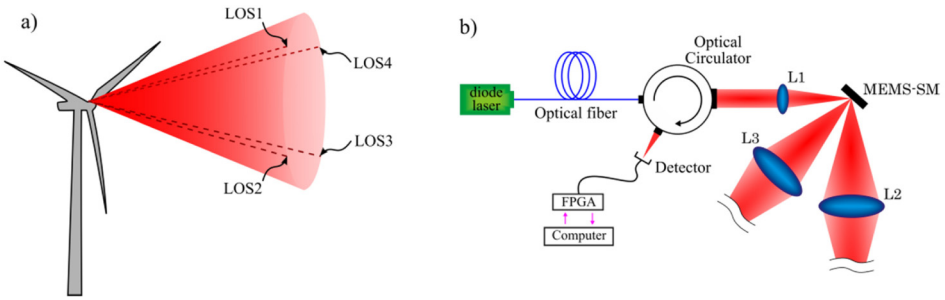

Fig. 1. (a) Geometry of the four lines-of-sight (LOS) of the lidar. The half cone angle is 18°. LOS1, LOS2, LOS3 and LOS4 represent the optical axes of four optical transceivers. On each LOS, the lidar beam is focused at a probing distance R = 60 m resulting in a Rayleigh length of 5 m. The beam is alternately focused to positions that form the vertices of a square. (b) Schematic of a multiple LOS (time-shared) lidar based on a MEMS-SM. The custom-built optical circulator consists of a polarizing beam splitter plate and a 45-degree Faraday rotator. The collimated output of the circulator has a beam diameter of 2 mm. For brevity, only two optical transceivers are shown in the sketch. L1: aspheric lens (f_1 = 8 mm). L2 and L3: 3-inch diameter doublet lenses ($f_2 = f_3$ = 216 mm).

The proposed lidar uses a dual-axis MEMS-SM (mirror diameter = 3 mm). Beam steering to multiple LOS relies on the 2D scanning feature of the MEMS-SM using its point-to-point scanning mode. The switch time between successive LOS impacts data availability and limits the effective acquisition rate – making it an important parameter to characterize. The MEMS-SM controller contains a low-pass filter (i.e. 6th order Bessel filter with a programmable cutoff frequency) for each axis drive input to reduce the mirror's mechanical oscillations that result from a step input signal [9]. In order to characterize the MEMS-SM switching speed, the time-domain step-response was measured for different low-pass cutoff frequencies ranging from 40 Hz to 200 Hz. The results are shown in Fig. 2(a). To make the measurement more precise, the optical power transmitted through the transceiver doublet lens is refocused by an identical lens into a ~1 mm on-axis pinhole at the focal plane in front of a detector as in Fig. 2(b). Optical power fluctuations caused by the mirror oscillations in response to a step input are sufficiently reduced to within ±3% of the steady-state (high) value at a cutoff frequency of 80 Hz or less.

#255741 Received 16 Dec 2015; revised 19 Jan 2016; accepted 21 Jan 2016; published 25 Jan 2016

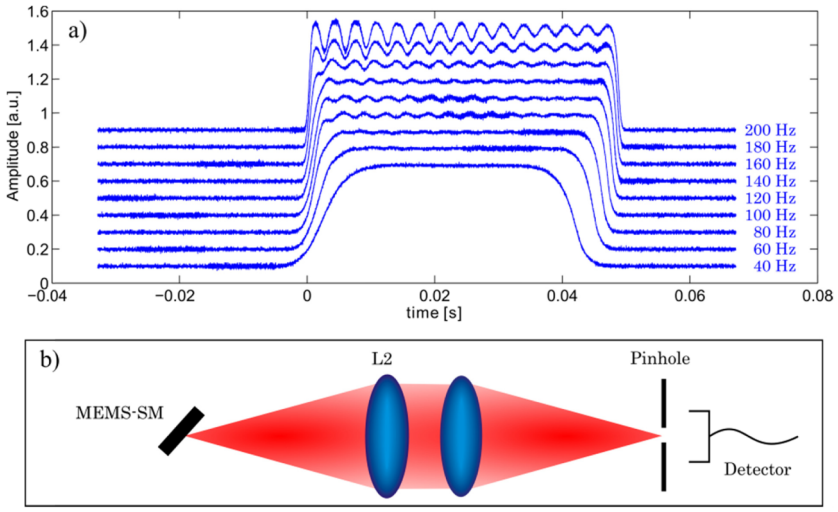

Fig. 2. (a) Step-response of the MEMS-SM for different input low-pass filter cutoff frequencies. For clarity, amplitude offsets of 0.1 to 0.9 are introduced to separate the curves. The amplitude represents the relative optical power the MEMS-SM is able to send through one doublet lens (e.g. L2) as it steers the lidar beam to successive LOS. (b) The setup used to probe the step-response of the MEMS-SM. Here the LOS of lens L2 was used. An identical doublet lens was placed in front of lens L2 to direct the optical power to an on-axis pinhole and a detector.

Based on the results in Fig. 2(a), all the measurements in the following sections were conducted using a filter cutoff frequency of 80 Hz, which gives a rise time and fall time of 3.85 ms and 2.63 ms, respectively. Rise and fall times are defined as the temporal duration between 10% and 90% of the steady-state amplitude.

3. Radial speed measurements with 4 lines-of-sight

Field test for outdoor wind measurement is conducted using the 4-LOS lidar. The raw wind spectra – i.e. PSD but with the frequency axis converted to speed using Eq. (1) – are produced from 512-point fast Fourier transform (FFT) of the photodetector signal at a sample rate of 100 MHz. Figure 3(a) shows the 50 Hz averaged wind spectra as a function of time. The color intensity represents the normalized Doppler signal strength (i.e. the noise floor is unity). The staircase feature in the data (evident in the first few seconds) demonstrates that we are indeed measuring the wind in all four LOS in a time-shared fashion.

Each vertical trace in Fig. 3(a) corresponds to a 50 Hz wind spectrum. Background noise measurements, shown in Fig. 3(b), were recorded by blocking the lidar beam. During the transition between two LOS, the spurious backreflection from the metallic material separating the doublet lenses is observed to cause a large signal peak at zero speed as seen in Fig. 3(b) and Fig. 3(c). In both cases, the recorded spectra immediately before (blue) and after (green) the transition spectra are shown. As observed, there are no signs of spurious peak in these spectra. This suggests that the switching time is indeed shorter than the 20 ms duration required to produce one averaged wind spectrum. The result agrees well with the MEMS-SM characterization shown in Fig. 2(a).

#255741 Received 16 Dec 2015; revised 19 Jan 2016; accepted 21 Jan 2016; published 25 Jan 2016

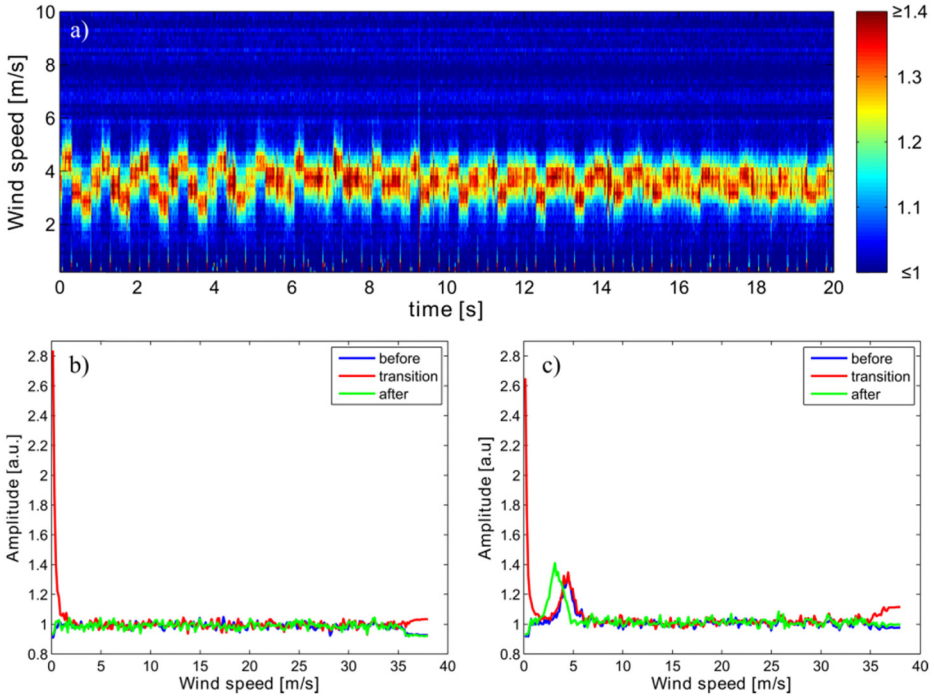

Fig. 3. (a) Sample wind spectra over 20 seconds at 50 Hz update rate. The color scale to the right denotes the Doppler signal strength normalized by the local oscillator dominated noise floor. (b) The background spectra of the lidar system when the probe beam is blocked. (c) Wind measured by the system before, during, and after a LOS transition. The red curves in (b) and (c) are the transition spectra between two LOS, while the blue curves are the spectra just before the transition and the green curves are the ones immediately after the transition.

As shown in Fig. 3(a), it is possible to visually discriminate the four LOS speeds while there are also occurrences where the radial speeds are similar to each other. Thus, further data processing is needed before the data is practically useful. An average wind speed is extracted from each 50 Hz wind spectrum using a simple peak-finding algorithm. The results are shown in Fig. 4. Since the data acquisition is not synchronized with the MEMS-SM steering control, the transition spectra can be either at the beginning or the end of each LOS data block. For this reason both the first and the last data point in each 0.25 s block are discarded, and the remaining data (i.e. about 80% duty cycle) are average into 1 Hz wind data for each LOS. The processed 1 Hz wind data are also presented in Fig. 4. It is also evident from Fig. 4, that discarding the transition spectra is necessary to avoid errors. Note that future synchronization of data acquisition and steering control, and the use of a peak-finding algorithm that discards spurious peaks in wind spectra can increase the duty cycle or data availability of the system.

#255741 Received 16 Dec 2015; revised 19 Jan 2016; accepted 21 Jan 2016; published 25 Jan 2016

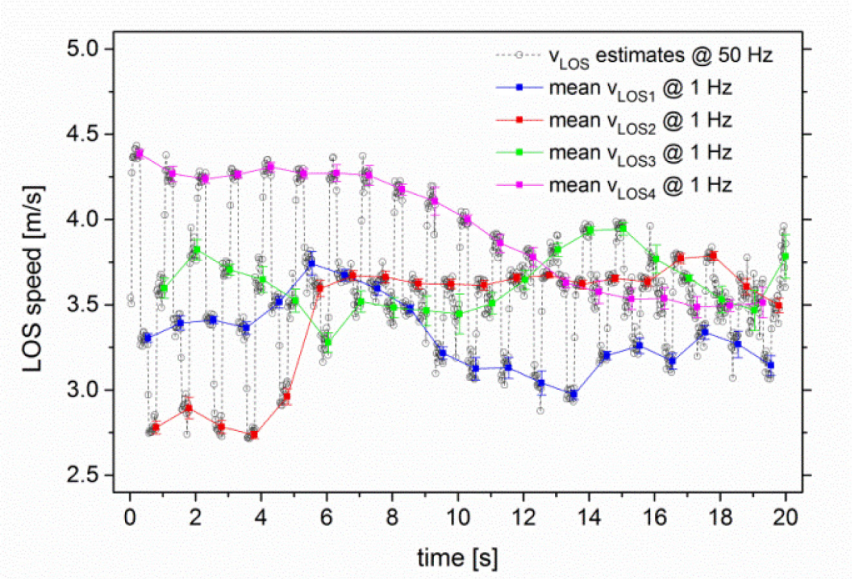

Fig. 4. The gray curve represents the wind data generated directly from the raw data in Fig. 3(a) using a LabVIEW peak-finding algorithm. The other curves represent the average radial wind speed in the four respective LOS where each data point is an average of 10 to 11 points from the 50 Hz radial speed data but excluding potentially erroneous data that correspond to transition spectra like the one shown in Fig. 3(c).

4. Spatial dithering to reduce the average irradiance of beam focus

In this section, we describe another elegant utility of the MEMS-SM that improves the ability of our lidar system to satisfy eye-safety requirements. The method relies on the active spatial dithering of the focused beam at a remote range *R* (tens of meters or more) so that it wanders over a larger area and effectively reduces the time-averaged irradiance (and hence the averaged energy density) during the exposure time. Since the needed area over which the beam is spatially dithered is much smaller in dimension compared to *R*, the influence of dithering on the radial speed measured by the lidar is extremely small and thus negligible.

A spatial dithering method has been conceptually proposed in a patent [10] but does not specifically disclose the use of a MEMS-SM. The optical geometry we propose here is also different. As shown in Fig. 5, the MEMS-SM is placed between the two telescope lenses of each optical transceiver (e.g. between L1 and L2). Furthermore, we describe how the MEMS-SM is able to apply a sufficient amount of spatial dither using a ray transfer matrix model.

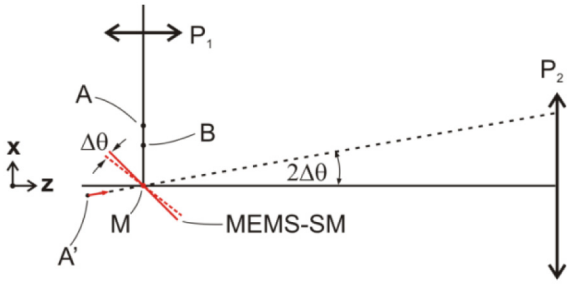

Fig. 5. Schematic diagram showing the relative positions of the MEMS-SM plane, planes P_1 and P_2 of lenses L1 and L2, respectively. Point A is where a collimated input beam is focused by lens L1. Point B indicates the focal point of lens L2. By pivoting at point M, the mirror deflects the beam either aligned with the optical axis of L2 or off-axis.

#255741 Received 16 Dec 2015; revised 19 Jan 2016; accepted 21 Jan 2016; published 25 Jan 2016

Consider the optical geometry in Fig. 5, which takes the case of the LOS defined by the optical axis of lens L2 in Fig. 1. Planes P_1 and P_2 indicate the locations of lens L1 and L2, respectively. An input collimated beam gets focused by lens L1at point A displaced from the focal point B of lens L2. An image of this focus at a far distance R to the right of plane P_2 is formed by lens L2 where the object distance is $\left(f_2 + \overline{\mathrm{AB}}\right)$ where $\overline{\mathrm{AB}} << f_2$. The thin lens formula gives the approximate image distance R for the object (focus) at point A for the optimally aligned case where $\Delta\theta = 0$, that is, the input ray vector is $(0, 0)$. If spatial dithering is applied, a small angular deflection $\Delta\theta$ of the mirror is introduced. This corresponds to having the object originate from a virtual point A' in Fig. 5 (i.e. $\overline{\mathrm{AM}} = \overline{\mathrm{A'M}}$) with an input ray vector $\left(-2\overline{\mathrm{AM}}\Delta\theta,\ 2\Delta\theta\right)$. Using ray transfer matrix analysis and assuming small mirror deflection $\Delta\theta$ and $R >> f_2$, the lateral displacement r_{out} at R is calculated as:

$$r_{out} = \left(x_{out}^2 + y_{out}^2\right)^{1/2} = \frac{2R\overline{\mathrm{AM}}}{f_2}\Delta\theta. \qquad (2)$$

Note that as $\overline{\mathrm{AM}} \to 0$ or as the beam focus is brought closer to M, $r_{out} \to 0$, which emphasizes our design criterion that the beam focus formed by lens L1 must not lie on the scanning mirror surface. $\overline{\mathrm{AM}}$ also has an upper limit that increases with the diameter of the scanning mirror used. For a given mirror diameter, $\overline{\mathrm{AM}}$ must not be too large in order to avoid significant beam truncation.

For the settings we used where R = 60 m, $\overline{\mathrm{MP_2}}$ = 212 mm and $\overline{\mathrm{BM}}$ = 4 mm, we find $\overline{\mathrm{AM}} = \overline{\mathrm{AB}} + \overline{\mathrm{BM}}$ = 4.78 mm. This is a sufficient value that avoids undesirable truncation of the beam incident on the mirror and results in a satisfactory $r_{out}/\Delta\theta$ ratio of 2.7 mm/mrad (for f_2 = 216 mm). This enables us to spatially dither the beam using a spiral trajectory shown in Fig. 6(a) over a circular region of 7 mm radius with a maximum mirror deflection of only 0.15 degree. Before applying spatial dither, the on-axis beam focused at R is approximately described by a Gaussian irradiance profile of radius ω_0 = 1.56 mm (measured by a beam profiler) as shown in Fig. 6(b). To estimate the effective irradiance for the spatially dithered case, we calculated the sum of Gaussian profiles each centered on coordinate points of the spiral trajectory divided by the number of Gaussians. The result shown in Fig. 6(c) illustrates that the mean irradiance resulting from spatial dithering is 40 times less than that at the center of a stationary beam. The initial frame of a short movie clip of the focused beam at R = 60 m being scanned in a spiral pattern is shown in Fig. 7. This result illustrates the potential to reduce the mean irradiance using a MEMS-SM based dithering method.

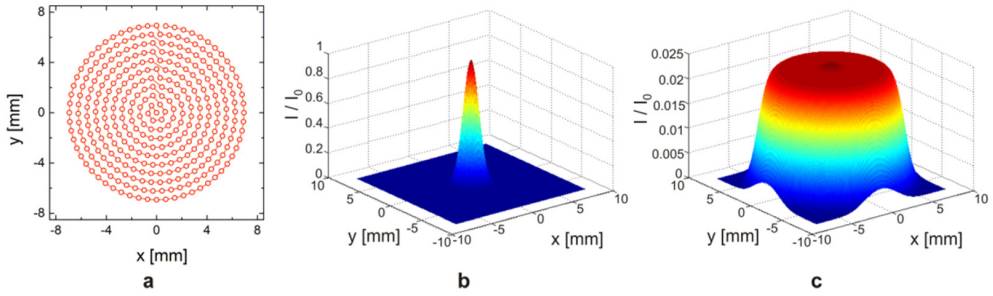

Fig. 6. (a) Spiral trajectory used for spatial dithering of the beam on the *xy*-plane. Simulated mean irradiance profiles at R = 60 m for the case (b) before, and (c) after applying the spatial dither. I_0 is the peak irradiance of the stationary Gaussian beam.

#255741 Received 16 Dec 2015; revised 19 Jan 2016; accepted 21 Jan 2016; published 25 Jan 2016

Fig. 7. First video frame of the spatially dithered focused beam (ω_0 = 1.56 mm) at probe range R = 60 m. The video (see Visualization 1) is slowed down four times the original speed to show the beam's spiral trajectory.

5. Robustness of the MEMS-SM

The manufacturer specified operating temperature of the dual-axis MEMS-SM is –40 °C to + 120 °C. However, its superb positional repeatability of 0.0005° is only specified at room temperature. In our current optical configuration with the probing beam focus at 60 m and $r_{out}/\Delta\theta$ ratio of 2.7 mm/mrad, the specified positional repeatability corresponds to a transverse position accuracy of 24 μm for the remote beam focus. The effect of large ambient temperature variation on this positional performance remains to be tested. Nevertheless, the lidar head housing that encapsulates the MEMS-SM together with other optical components contains a temperature sensor and heating elements to enable a rudimentary regulation of the enclosure's internal temperature (room temperature ± 5 °C) for most outdoor conditions.

According to specifications, the Al or Au coated mirror of the MEMS device can handle incident optical powers up to 1 W across a broad wavelength range. Although a specification of damage threshold in units of W/cm^2 is needed to assess an incident beam of specific width or profile, we consider the 500 mW laser power (at 1.5 μm wavelength) used in our system to be below the limit. This is validated by the fact that no laser induced thermal effects on the MEMS-SM were observed. As also described in the previous section, the laser beam is, by design, focused at a finite distance from the mirror surface to achieve an adequate $r_{out}/\Delta\theta$ ratio for spatial dithering – effectively reducing the power density of the incident beam on the mirror surface. Furthermore, the lidar head enclosure prevents or minimizes dust contamination to the MEMS-SM.

In contrast to bulk mechanical beam-scanners (e.g. Risley prisms or galvanometer scanning mirrors), the MEMS-SM has a dynamic component that is more robust to wear and tear due its ultra-low mass. MEMS-SM offers other advantages due to its mass-producible and low-power consumption features. With a typical specification of >1 billion switch cycles, the MEMS-SM has a projected lifetime of a few decades – matching the operational lifespan of a wind turbine.

6. Conclusion

We have demonstrated a novel semiconductor laser wind lidar with four time-shared lines-of-sight based on a MEMS-SM device. Radial wind speed data obtained from a field test have been presented, and it is clear that speed components along four LOS are distinguishable. Characterization of the MEMS-SM shows that the temporal step-response of the device is fast enough to satisfy our target radial speed acquisition rate of 50 Hz, which is relevant for applications such as wind turbine blade pitch control. Furthermore, we have demonstrated experimentally that the MEMS-SM is capable of spatially dithering the beam at the desired focal plane (at 60 m remote distance in our demonstration). This reduces the mean irradiance of the lidar probe beam at the focal plane – relevant for meeting eye-safety requirements. It is

#255741 Received 16 Dec 2015; revised 19 Jan 2016; accepted 21 Jan 2016; published 25 Jan 2016

also worth noting that unlike the liquid-crystal based beam steering method, the use of MEMS-SM enables steering of an incident beam of any polarization state and any wavelength over a wide spectral range – features that have potential advantages in future variants of our lidar system. These include future designs that aim to further increase the number of measurement points to achieve a more detailed measurement of wind profiles by increasing the number optical transceivers used. As we mentioned in the first section, this will be constrained by the size of the optics. Note however that if a shorter wavelength is used with a MEMS-SM for beam steering and dithering, smaller focusing lenses can be utilized while keeping the same spatial resolution since Rayleigh length scales inversely with wavelength.

Acknowledgment

The authors are grateful for the financial support from the Energiteknologisk Udviklings- og Demonstrations Program (EUDP) J.nr. 64014-0160.

#255741 Received 16 Dec 2015; revised 19 Jan 2016; accepted 21 Jan 2016; published 25 Jan 2016